RSC Advances

PAPER

View Article Online
View Journal | View Issue

Cite this: *RSC Adv.*, 2026, **16**, 30526

Transition metal-induced excess electron localization driving the giant first hyperpolarizability in alkaline earthides: a DFT and TD-DFT study

Jabir Hussain, *[a] Riaz Hussain, *[b] Dua Tahreem,[b] Annum Ahsan,[c] Muhammad Arshad [a] and Khurshid Ayub [c]

The rational design of alkaline earthides with high stability and superior nonlinear (NLO) response remains a significant challenge. In this work, 3d transition metals (V–Zn) are used for the first time as donors of excess electrons to develop a series of earthides, *i.e.*, $M^+(3^6adz)Ca^-$ (M^+ = V–Zn), using 3^6adz as the complexant. Density functional theory (DFT) calculations were carried out using the ωB97X-D functional along with the 6-31 G+(d,p) basis set to investigate their electronic and NLO properties. All the complexes exhibit high thermal stability compared with previously reported earthides, with interaction energies ranging from −12.10 to −117.7 kcal mol^{-1}. Natural bond orbital and frontier molecular orbital analyses show negative charge and HOMO density over the Ca metal, validating their earthide nature. The studied complexes show exceptional NLO response with enhanced first hyperpolarizability (β_o) values up to 3.17×10^6 a.u. for $Zn^+(3^6adz)Ca^-$. The high β_o values of the complexes are attributed to the position of the excess electrons in the p-orbital of the Ca metal, which is confirmed through the partial density of state spectra. The β_o values of the complexes are further rationalized using two-level model analysis. The earthides possess small transition energies ranging from 0.67 to 2.28 eV along with reduced energy gaps. Moreover, the application of an external electric field (EEF) further increases their β_o values. Notably, the β_o value of $Zn^+(3^6adz)Ca^-$ increases from 3.17×10^6 to 1.25×10^7 a.u. under an EEF strength of 0.001 a.u. This work introduces a new strategy for designing alkaline earthides using transition metals as a donor of excess electrons and will encourage experimental efforts toward the synthesis of stable earthides.

Received 18th March 2026
Accepted 15th May 2026

DOI: 10.1039/d6ra02261h

rsc.li/rsc-advances

1. Introduction

The increasing number of applications of nonlinear optical (NLO) materials in optical communication,[1] laser devices,[2] and photo-catalysis,[3] *etc.*, has urged scientists to design materials with excellent NLO responses.[4–9] Various strategies have been adopted to introduce nonlinear optical behavior in a wide range of materials. These strategies include diradical characters,[10,11] donor-π-acceptor systems,[12] octupolar molecule synthesis,[13] and excess electron-containing systems.[14–21] In 2004, Li *et al.* reported that the systems containing excess electrons showed excellent NLO responses.[22,23] After that, the introduction of excess electrons in a material has been regarded as an admirable strategy for enhancing the NLO response. A variety of materials with inserted excess electrons have been proposed and reported. The electrides[24–26] were the first class of excess electron-containing materials reported in the literature with huge NLO responses. Their design involves the encapsulation of an alkali metal inside the complexant to serve as a donor of excess electrons. The excess electrons in the complexes act as anions and spread over the complexant, producing a negative charge over it. The Cs^+(18-crown-6)$2e^-$ was the first electride reported in the literature; it contains an 18-crown-6 ether complexant with Cs as an excess electron donor.[27] Moreover, M^+(cryptand [2.2.2])e^- has also been investigated as an electride with the cryptand[2.2.2] as the complexant and alkali metals (Li–K) as the excess electron sources.[28] After that, many electrides with different complexants and electron donors have been reported[29–33] in the literature to date.

Another versatile class of excess-electron systems is alkalides, which exhibit improved NLO response. These are designed by inserting alkali metals (AMs) inside the complexant

[a]*Institute of Chemistry, The Islamia University of Bahawalpur, Bahawalpur, 63100, Pakistan. E-mail: chemistjabir@gmail.com; muhammad.arshad@iub.edu.pk; Tel: +92-3428579289*

[b]*Division of Science and Technology, Department of chemistry, University of Education Lahore, Campus D.G khan, Dera Ghazi khan, 32200, Pakistan. E-mail: duatahreem06@gmail.com; riaz.hussain@ue.edu.pk; Tel: +92-3336364880*

[c]*Department of Chemistry, COMSATS University, Abbottabad Campus, Abbottabad, 22060, Pakistan. E-mail: annumahsan12@gmail.com; khurshid@cuiatd.edu.pk*

as an excess electron donor for alkali metals that are placed on the outer face of the cage. Thus, the alkali metal present outside the complexant changes into an alkali metal anion,[34–38] *i.e.*, M^+(calix[4]pyrrole)M^-[39] and M^+(n^6adz)M^-,[40] in which the alkali metals act as anions and cations, respectively.

Recently, a new type of complex, namely alkaline earthides, has been reported that shows enhanced NLO response compared to the previous classes of excess-electron systems. In these complexes, the AMs act as the donor and the alkaline earth metal (AEMs) act as the acceptor of excess electrons. These are designed by intercalating AMs inside the complexant and AEMs on the outer face of the complexant. For the first time, alkaline earthides are reported by using $C_6H_6F_6$ complexant, *i.e.*, Li($C_6H_6F_6$)M (where M can be Be–Ca metal acting as electron acceptors).[41] The alkaline earthides have been a topic of significant interest to our research group over the past few years, and several systems have been reported.[42–47] All the reported earthides possess exceptional nonlinear optical responses, which inspired us to study them further. Notably, previously reported earthide complexes utilized AMs as donors of excess electrons. However, transition metals (TMs), which possess multiple valence electrons, have not yet been extensively explored as donors in excess-electron systems. To address the gap, we investigated the behavior of TMs as excess electron donors. We selected 3^6adz (complexant) to design earthide complexes due to its large cavity, which provides a favorable environment in which to occupy the TMs. It is a cyclic organic molecule containing nitrogen atoms along with carbon and hydrogen atoms. Previous studies showed that earthides designed using 3^6adz and alkali metals as donors of excess electrons exhibit remarkable NLO responses.[42,48–50] For this reason, we selected the 3^6adz (admanzene) and propose a new series of earthides complexes with high NLO response and stability. The design principle involves placing TMs (V–Zn) inside and Ca metal outside the complexant. The nitrogen atoms surround the TMs at a specific distance (as shown in Fig. 1). The novelty is that, in these complexes, transition-metal atoms (V–Zn) are used as an excess electron source, and Ca metal is used as an electron acceptor.

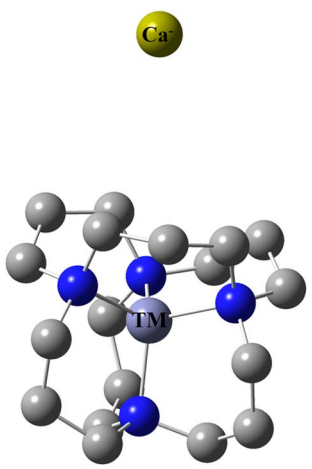

Fig. 1 Stable 3D structure of the M^+(3^6adz)Ca^- (M^+ = V–Zn) series with hydrogen atoms omitted.

2. Computational methodology

In the present study, the long-range, hybrid functional ωB97X-D was employed to carry out all the analyses. Literature studies show that it is the best functional level for studying complexes containing alkali and alkaline earth metals.[51] It produces precise results to study thermochemistry, non-covalent bonding, and transfer of charge in components of complexes.[43,52,53] In the current study, charge transfer among the constituents of the complexes and long-range interactions are prime features of the complexes. These required a long-range functional for accurate analysis of their properties. The ωB97X-D was selected and used with the 6-31G+(d,p) basis set to carry out all calculations. Furthermore, previously reported studies have shown that NLO results calculated using ωB97X-D are comparable to those estimated using the coupled-cluster method, which is considered a better method in quantum chemistry.[54] Historically, it is employed for the precise measurement of hyperpolarizability and polarizability. However, its usage is limited due to high computational cost. On the other hand, density functional theory offers a balance between computational cost and accuracy of results. So, it has gained huge attention from researchers due to its reduced computational cost and high accuracy in results. However, the hyperpolarizability calculated by the DFT method is functional-dependent, mainly due to the exchange correlation in each function. The complexes under investigation are large, for which CCSD (*T*) calculations are not possible. So, on the basis of results obtained after a comparison study with CCSD(T), DFT methods were selected for the current study. A literature survey shows that a functional with range separation is required for accurate investigation of the hyperpolarizability of complexes. So, the ωB97X D functional was selected as it is functional with 100% long-range.[25,55–60] All the DFT-based calculations were carried out with Gaussian 09 software,[61] and the results are displayed using the GaussView 5.0 package.[62] All calculations were performed using the default isotopic masses as implemented in Gaussian 09, corresponding to the most abundant natural isotopes (^{51}V, ^{52}Cr, ^{55}Mn, ^{56}Fe, ^{59}Co, ^{58}Ni, ^{63}Cu, ^{64}Zn, and ^{40}Ca).[63] The presence of true minima was verified by the absence of an imaginary frequency in the calculated vibrational frequencies.

First, the geometries of the complexes were optimized using ωB97X-D and the 6-31 G+(d,p) basis set. The thermal stability of the optimized complexes was evaluated by measuring the values of their interaction energies (E_{int}) through eqn (1). While the stability related to the electron was estimated by calculating the vertical ionization potential (VIP) through eqn (2).

$$E_{int} = E_{M+(36adz)Ca^-} - [E_{TMs} + E_{Ca} + E_{36adz}] \quad (1)$$

$$VIP = -E_{HOMO} \quad (2)$$

To account for basis set superposition error (BSSE) in the interaction energy calculations, the counterpoise correction method was employed. The BSSE-corrected interaction energies were calculated for the designed earthide complexes using the

same level of theory adopted for the geometry optimizations and energy calculations.

After that, electronic parameters, including NBO (natural bond orbitals) charge analysis,[64] position of the HOMO (highest occupied molecular orbital) and energy gap (E_{H-L} gaps) between the HOMO and LUMO (eqn (3)), were investigated.[65] Furthermore, the partial density of states (PDOS) spectra were drawn by employing Multiwfn software to verify the position of the HOMO in the complexes.[66] For the detailed study, dipole moments (μ_o), polarizability (α_o), first hyperpolarizability (β_o), and hyperpolarizability projection along the dipole vector were analyzed using eqn (4)–(7) a, respectively.

$$E_g = E_H - E_L \quad (3)$$

$$\mu_0 = \sqrt{\mu_x^2 + \mu_y^2 + \mu_z^2} \quad (4)$$

$$\alpha_0 = \frac{1}{3}(\alpha_{xx} + \alpha_{yy} + \alpha_{zz}) \quad (5)$$

$$\beta_0 = \sqrt{(\beta_{xxx} + \beta_{xyy} + \beta_{xzz})^2 + (\beta_{yyy} + \beta_{yzz} + \beta_{yxx})^2 + (\beta_{zzz} + \beta_{zxx} + \beta_{zyy})^2} \quad (6)$$

$$\beta_{vec} = \sum \frac{\mu_i \beta_i}{|\mu|} \quad (7)$$

After that, time-dependent DFT analysis was carried out in order to figure out the oscillator strength (f_o), transition energies (ΔE) and variations in dipole moment ($\Delta\mu$) by using the same level of theory.[67–70] The UV-visible graph was generated to show the ultra-transparency of the complexes. Additionally, the increase in the NLO response of the complexes after the application of an external electric field (EEF) of 10^{-3} a.u. strength was analyzed by repeating the same calculations, *i.e.*, optimization, NBO charge study, hyperpolarizability and energy gap analysis. The EEF was applied in a direction similar to that of the charge transfer and its opposite. It is expected that the EEF will help to improve the NLO properties of the proposed system.

3. Results and discussion

3.1. Analysis of geometrical properties and thermal stability

The complexes of the $M^+(3^6adz)Ca^-$ (M^+ = V–Zn) series involved a TM as a donor of excess electrons and Ca metal as an acceptor of excess electrons. The TMs have the issue of spin multiplicity because of the possibility of variable stable spin states. Therefore, to evaluate the most stable spin state of the complexes, the designed geometries were optimized at the ωB97X-D/6-31+G(d,p) level of theory, considering the four lowest spin states. Due to even/odd electrons fluctuation, each complex has a different stable spin state. The stable spin state of each complex is presented in Fig. 3.

The optimized structures (presented in Fig. 2(a) and (b)) contain TMs inside the 3^6adz (complexant) and a Ca metal outside of 3^6adz, interacting with hydrogen atoms of the cage. Each $M^+(3^6adz)Ca^-$ complex consists of a transition-metal atom encapsulated inside the 3^6adz cage, while the Ca atom is positioned outside the cage. The transition metal interacts with the nitrogen atoms of the cage, whereas the Ca atom interacts primarily with the hydrogen atoms on the outer surface. This arrangement facilitates charge transfer from the encapsulated metal to the external Ca atom, resulting in electron localization on Ca and confirming the earthide nature of these complexes. The overall geometry is stabilized through non-covalent interactions between the metal centers and the ligand framework. The interaction distances between the TMs and Ca metal in the optimized geometries were calculated and are presented in Table 1. The results revealed that interaction distance changes in the nonlinear pattern from $V^+(3^6adz)Ca^-$ to $Zn^+(3^6adz)Ca^-$ due to the non-monotonic change in size and number of available electrons in the TM from V to Zn. As only Ca metal is used as an acceptor metal in all the designed complexes, so the interaction distance depends greatly upon the size of the donor metal (V to Zn). The interaction distance is observed in order $V^+(3^6adz)Ca^-$ (5.38 Å) < $Mn^+(3^6adz)Ca^-$ (5.75 Å) < $Zn^+(3^6adz)Ca^-$ (5.90 Å) < $Co^+(3^6adz)Ca^-$ (5.95 Å) = $Ni^+(3^6adz)Ca^-$ (5.95 Å) < $Cu^+(3^6adz)Ca^-$ (5.99 Å). Interestingly, similar interaction distances are seen for $Co^+(3^6adz)Ca^-$ and $Ni^+(3^6adz)Ca^-$ complexes, as well as for $Cr^+(3^6adz)Ca^-$ and $Fe^+(3^6adz)Ca^-$ complexes, despite variations in their atomic sizes and electronic configurations. This shows that the interaction distance is not controlled solely by atomic size, but also by electronic factors, such as d-orbital occupancy, effective nuclear charge, and the extent of charge transfer. The comparable distances can be attributed to similar electronic environments and charge-transfer characteristics, as supported by the NBO analysis. Moreover, the greater distance between Cu and Ca in $Cu^+(3^6adz)Ca^-$ is due to the completely occupied 3d-orbital of the Cu metal, which makes the core around the nucleus and repels the 4s-orbital electron, so the size of Cu increases, which pushes away the electrons of the Ca metal. For this reason, the interaction distance between the Cu and Ca metals in the complex increases. On the other hand, the shorter distance between the TM and Ca metals in $V^+(3^6adz)Ca^-$ is due to the presence of the valence electrons of vanadium metal in lower d-orbitals, which exhibits less repulsion to Ca and results in a reduced distance between both metals. Additionally, the vanadium metal has a small size and unpaired electrons, which attract the calcium metal significantly, resulting in a lower interaction distance.

Additionally, the interaction energy (E_{int}) values of the studied complexes were calculated using eqn (1) and are presented in Table 1 to evaluate the thermodynamic stability of the

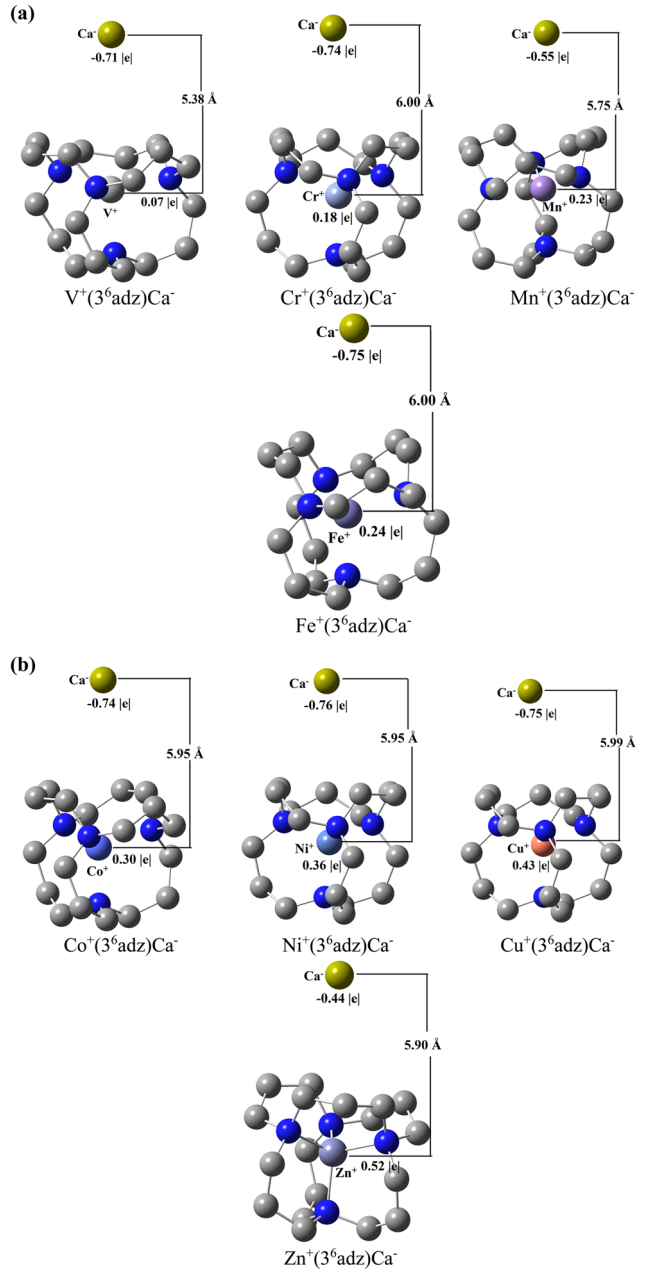

Fig. 2 (a). Optimized structures of the complexes of $M^{+}(\bar{3}^{6}adz)Ca^{-}$ (M^{+} = V–Fe) after removing the hydrogen atoms and with the calculated distances between their inner and outer metals. (b). Optimized structures of the complexes of $M^{+}(\bar{3}^{6}adz)Ca^{-}$ (M^{+} = Co–Zn) after removing the hydrogen atoms and with the calculated distances between their inner and outer metals.

optimized geometries. All the complexes are thermodynamically stable, as determined by their E_{int} values (observed in the range of −12.10 to −117.7 kcal mol^{-1}). It was found that E_{int} is greatly affected by the size of the TMs as well as the size of the Ca metal. The size of the Ca metal is large, which makes it more reactive in complex formation. For this reason, the complexes have greater interaction energies. All the complexes have negative interaction energies, confirming that the complex formation is exothermic and produces stable complexes. In the studied complexes, the highest interaction energy observed for the $Cr^{+}(3^{6}adz)Ca^{-}$ complex is attributed to enhanced charge transfer and effective orbital interaction. Although both Cr and Mn possess a d^{5} configuration, Cr ($3d^{5}4s^{1}$) has more accessible valence electron density, which facilitates stronger interaction with the Ca atom. This is supported by NBO analysis, where greater charge transfer is observed in the Cr complex compared to Mn. In contrast, Mn ($3d^{5}4\ s^{2}$) exhibits a relatively stable electronic configuration, resulting in reduced electron donation and weaker interaction energy.

The lowest value is noted for the $Zn^{+}(3^{6}adz)Ca^{-}$ (−12.10 kcal mol^{-1}) complex due to the completely filled 3d orbital electrons of the Zn metal, which reduces the interaction of the metal with the cage atoms and results in a lower interaction value. The investigated complexes are composed of fragments, so the basis set superposition error (BSSE) corrected interaction energies ($E_{int(BSSE)}$) were determined, as shown in Table 1. The BSSE-corrected interaction energies involved the encapsulation of metals, ranging from −90.13 to −2.37 kcal mol^{-1}. The results show that $E_{int(BSSE)}$ is altered as compared to the uncorrected interaction energies. But the overall negative values show the exothermic interaction between the metals and the complexant.

3.2. Nature of the earthides and electronic stability analysis

The studied complexes belong to the class of alkaline earthides, in which excess electrons are transferred from the encapsulated transition metal toward the outer Ca atom, leading to electron localization on Ca. In this context, the notation $M^{+}(3^{6}adz)Ca^{-}$ is used to represent the direction of charge transfer, rather than formal oxidation states. The charge distribution is quantified using NBO analysis, which reveals a partial positive charge on the transition metal and a negative charge on Ca. Due to the delocalized nature of the electron density and the strong charge-transfer interactions in these systems, assigning integer oxidation states is not appropriate. Therefore, the electronic structure is more accurately described in terms of charge transfer and orbital localization rather than formal oxidation states.

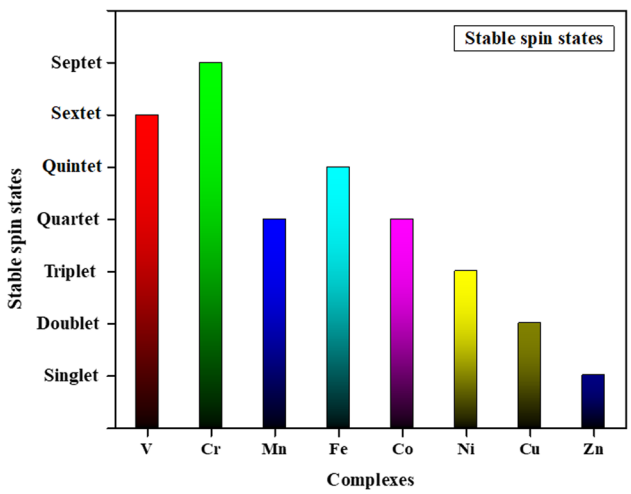

Fig. 3 Stable spin states of the TMs in the Ca series of the complexes.

Table 1 NBO charges on M^+ and Ca^- represented by $Q_{M}{}^{+}$ and $Q_{Ca}{}^{-}$ in $|e|$, symmetries, vertical ionization potential (VIP) in eV, interaction energies (E_{int}) in kcal mol^{-1}, basis set superposition error (BSSE)-corrected interaction energies ($E_{int(BSSE)}$), average distances between the metals ($d_{M}{}^{+}{}_{-Ca}{}^{-}$) in Å, dipole moment ($\mu_o$) in D, and energies of HOMO (E_H), LUMO (E_L) and their corresponding gap (E_g) in eV of the $M^+(3^6adz)Ca^-$ complexes

$M^+(3^6adz)Ca^-$	$Q_{M}{}^{+}$	$Q_{Ca}{}^{-}$	S_{ym}	VIP	E_{int}	$E_{int(BSSE)}$	$d_{M+-Ca}{}^{-}$	μ_o	E_H	E_L	E_g
$V^+(3^6adz)Ca^-$	0.07	−0.71	C_1	2.33	−53.67	−27.87	5.38	19.46	−2.33	0.17	2.51
$Cr^+(3^6adz)Ca^-$	0.18	−0.74	C_1	2.29	−117.7	−90.13	6.00	21.31	−2.29	0.14	2.43
$Mn^+(3^6adz)Ca^-$	0.23	−0.55	C_1	2.51	−45.45	−14.98	5.75	10.57	−2.51	0.40	2.91
$Fe^+(3^6adz)Ca^-$	0.24	−0.75	C_1	2.28	−98.18	−77.72	6.00	21.36	−2.28	0.20	2.49
$Co^+(3^6adz)Ca^-$	0.30	−0.74	C_1	2.30	−95.27	−10.09	5.95	20.97	−2.30	0.25	2.55
$Ni^+(3^6adz)Ca^-$	0.36	−0.76	C_1	2.28	−72.69	−11.73	5.95	21.21	−2.28	0.25	2.54
$Cu^+(3^6adz)Ca^-$	0.43	−0.75	C_1	2.28	−25.55	−10.12	5.99	21.43	−2.28	0.20	2.48
$Zn^+(3^6adz)Ca^-$	0.52	−0.44	C_1	2.11	−12.10	−2.37	5.90	8.16	−2.11	−0.41	1.70

To explore the electronic properties, *i.e.*, charge transfer between both metal ions, and to verify the earthide characteristics of the $M^+(3^6adz)Ca^-$ (M^+ = V to Zn) complexes, NBO analysis was carried out.[71] The results of the NBO analysis, presented in Table 1, show that there is a negative charge on Ca in the studied complexes, which verifies the earthide character of the complexes. With a negative charge on the Ca metal, a positive charge is produced on the TMs, validating that charge transfer occurs from the TMs to the Ca metal. In this way, excess electrons that are added into the complexes reside over the acceptor metal in the system, *i.e.*, the Ca metal. The NBO analysis shows that the $M^+(3^6adz)Ca^-$ series follows a nonlinear trend in the increase of NBO charge on the acceptor metal (Ca metal). The trend observed in the NBO charges of the $M^+(3^6adz)Ca^-$ (M^+ = V to Zn) series is given as: $Ni^+(3^6adz)Ca^-$ (−0.76 $|e|$) > $Fe^+(3^6adz)Ca^-$ (−0.75 $|e|$) = $Cu^+(3^6adz)Ca^-$ (−0.75 $|e|$) > $Co^+(3^6adz)Ca^-$ (−0.74 $|e|$) = $Cr^+(3^6adz)Ca^-$ (−0.74 $|e|$) > $Zn^+(3^6adz)Ca^-$ (−0.44 $|e|$) > $Mn^+(3^6adz)Ca^-$ (−0.55 $|e|$). The greater negative charge observed on the Ca metal in the $Ni^+(3^6adz)Ca^-$ complex indicates the higher transfer of electrons from Ni to Ca metal. This occurs due to the d-electron-rich nature of the Ni metal, which participates in back electron donation. Additionally, the Ni and Ca interaction in the complex is highly polarized, with Ni metal acting as a Lewis base and Ca as a Lewis acid. Also, Ni metal is a d^8 electron system. All these characteristics result in a higher transfer of electrons towards the acceptor metal in the complexes. Lower electron transfer is observed in the $Mn^+(3^6adz)Ca^-$ complex towards the acceptor metal, which is because the Mn metal has a d^5 configuration (with common +2 oxidation state), which is a half-filled d-subshell. For this reason, Mn has less tendency to donate electrons and resists oxidation. Moreover, the electrons in the d-orbitals are tightly bound due to the effective nuclear charge, along with a high energy gap, which makes it less effective for back electron donation and ultimately results in less transfer of electrons towards the Ca metal and a decrease in the NBO charge value over the acceptor metal.

To further confirm the earthide nature of the complexes, FMO (frontier molecular orbitals) investigation was performed to examine the HOMO position in the complexes. The results revealed that, in all the complexes, the HOMO resides over the Ca metal (as shown in Fig. 4/S1) except for the $Mn^+(3^6adz)Ca^-$ complex, for which the HOMO resides over the complete geometry. This is because of the lower transfer of electrons from the donor metal (Mn metal) towards the acceptor metal because of the half-filled stable d-orbital, which makes the electrons more tightly bound to the nucleus. When the nitrogen atoms of the cage push the valence electrons of Mn metal, these are diffused over the structure instead of undergoing complete transfer. This verifies the earthide characteristics of the investigated complexes. The stable geometries of all the complexes contain TMs on the inner side of the cage and Ca metal interacting with hydrogen atoms lying on the outer face of the cage. The nitrogen atoms in the cage expel the valence electrons of the transition metal (V to Zn) outward due to their lone pairs, and the electron finally surrounds the Ca metal, which can be seen in the form of the HOMO. Additionally, the H–L energy gaps of the designed complexes were calculated in the FMO study,[72] and found to be very small (1.70 eV–2.91 eV) as compared to the pure cage's H–L energy gap, *i.e.*, 8.50 eV. The greater decline in value is attributed to the excess electrons present in these complexes. It is important to note that the $Zn^+(3^6adz)Ca^-$ complex exhibits a negative LUMO energy compared to the positive values observed for the other complexes. This unusual behavior is attributed to the enhanced stability of the acceptor orbital in the Zn system. The fully filled d^{10} electronic configuration of Zn leads to reduced inter-electronic repulsion and stronger orbital polarization effects, which significantly lower the energy of the LUMO level. As a result, the LUMO becomes more negative compared to other transition-metal complexes, leading to a negative value.

It is seen that the H–L gap in the $M^+(3^6adz)Ca^-$ series varies in a nonlinear pattern. The decreasing order of H–L gap is: $Mn^+(3^6adz)Ca^-$ (contain H–L gap of 2.91 eV) > $Co^+(3^6adz)Ca^-$ (2.55 eV) > $Ni^+(3^6adz)Ca^-$ (2.54 eV) > $V^+(3^6adz)Ca^-$ (2.51 eV) > $Fe^+(3^6adz)Ca^-$ (2.49 eV) > $Cu^+(3^6adz)Ca^-$ (2.48 eV) > $Cr^+(3^6adz)Ca^-$ (2.43 eV). This indicates the conducting behavior of the complexes. The higher energy gap is recorded for $Mn^+(3^6adz)Ca^-$ due to the d^5 system of the TM in it, which needs high energy to transfer electrons to the acceptor metal. This reduces the transfer of electrons towards the acceptor metal, which can be verified in the NBO results of the same complex. The lower energy gap recorded for the $Cr^+(3^6adz)Ca^-$ complex is due to the low-lying d-orbital in Cr metal, which interacts with the diffused

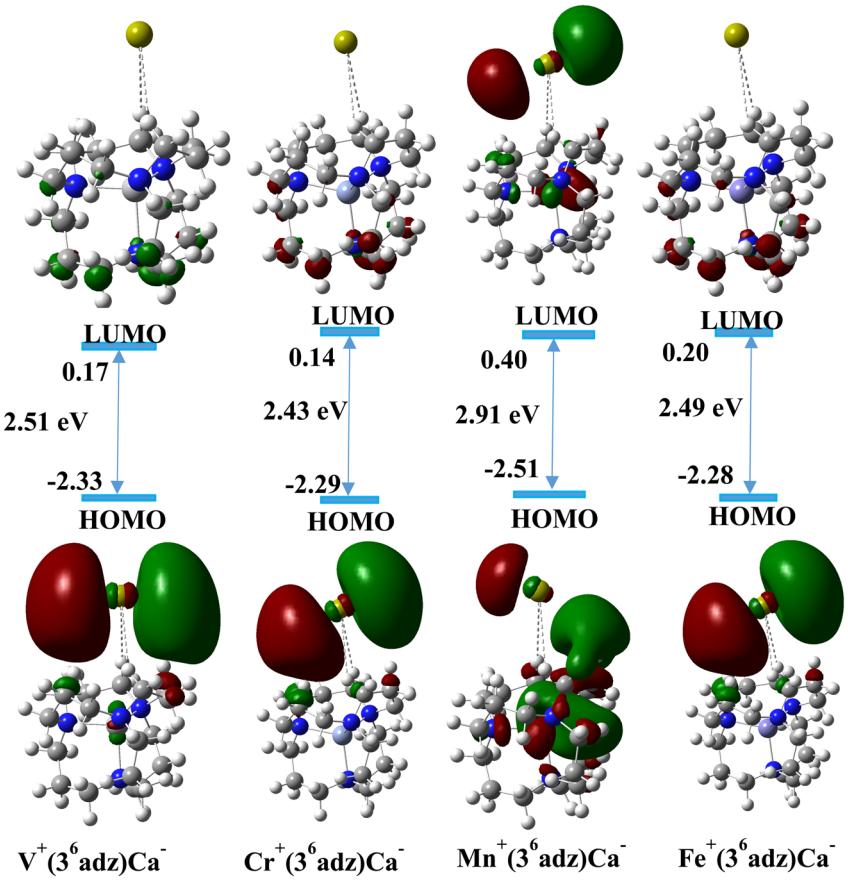

Fig. 4 HOMOs and LUMOs of $M^{+}(3^{6}adz)Ca^{-}$ generated at an isovalue of 0.02.

orbital of the Ca metal and leads to orbital hybridization. Additionally, the complex has a lower value for the LUMO energy, which narrows the energy gap of the complex. Even though the H–L gaps of the designed alkaline earthides are much reduced as compared to the parent complexant, 3^{6}adz (8.50 eV), the values of the H–L gaps are moderately high, which gives sufficient electronic stability to the complexes. Moreover, the PDOS (partial density of states spectra (Fig. 5 and S2); were generated to validate the position of the HOMO. All the spectra showed that the HOMO of all the designed complexes is present over the Ca metal. Moreover, the energy gaps of the complexes are also verified by the PDOS plots.

All the complexes possess significant VIP values (Table 1). Such high VIP values add electronic stability to the complexes. The series-wise analysis shows that it changes in an irregular pattern from $V^{+}(3^{6}adz)Ca^{-}$ to $Zn^{+}(3^{6}adz)Ca^{-}$ due to the nonlinear change in the H–L gap and the distance between the two metals in the complexes. Also, the size of the transition metals affects the VIP value. The trend in VIP is observed in order of $Mn^{+}(3^{6}adz)Ca^{-}$ (2.51 eV) > $V^{+}(3^{6}adz)Ca^{-}$ (2.33 eV) > $Co^{+}(3^{6}adz)Ca^{-}$ (2.30 eV) > $Cr^{+}(3^{6}adz)Ca^{-}$ (2.29 eV) > $Fe^{+}(3^{6}adz)Ca^{-}$ (2.28 eV) = $Ni^{+}(3^{6}adz)Ca^{-}$ (2.28 eV) > $Zn^{+}(3^{6}adz)Ca^{-}$ (1.70 eV). It is worth noting that the Ni and Cu complexes exhibit identical VIP values (Table 1). This arises from the very similar HOMO energies at the chosen level of theory. Minor differences exist beyond the reported decimal precision; however, rounding to two decimal places results in identical values.

3.2.1. Dipole moment investigation. The mean dipole moment (μ_o) of the complexes was calculated to gain insight into the electronic properties of the complexes, and their values are given in Table 1. The calculated significant μ_o values reveal the extent of charge separation in the studied earthide complexes, which play a prime role in the generation of the NLO response of the complexes. As the μ_o is a multiple of the quantity of charges and the distance between them, so both parameters directly control the μ_o values. The direct relationship of μ_o with the distance between the two charges can be seen in the μ_o values observed for the $M^{+}(3^{6}adz)Ca^{-}$ series. All the complexes show a triggering in the dipole moment with an enhancement of the distance between the two charged metals, and the NBO charges over the intercalated metals. A higher dipole moment is calculated for $Cu^{+}(3^{6}adz)Ca^{-}$ complex due to the larger interaction distance and the charge magnitude, along with the lower energy difference. On the other hand, a lower dipole moment is seen for $Zn^{+}(3^{6}adz)Ca^{-}$ due to the small charge value and the distance between the interacting metals. Overall, the trend of μ_o is observed as: $Cu^{+}(3^{6}adz)Ca^{-}$ (21.43 D) > $Fe^{+}(3^{6}adz)Ca^{-}$ (21.36 D) > $Cr^{+}(3^{6}adz)Ca^{-}$ (21.31 D) > $Ni^{+}(3^{6}adz)Ca^{-}$ (21.21 D) > $Co^{+}(3^{6}adz)Ca^{-}$ (20.97 D) > $V^{+}(3^{6}adz)Ca^{-}$(19.46 D) > $Mn^{+}(3^{6}adz)Ca^{-}$ (10.57 D) > $Zn^{+}(3^{6}adz)Ca^{-}$ (8.16 D). So, the

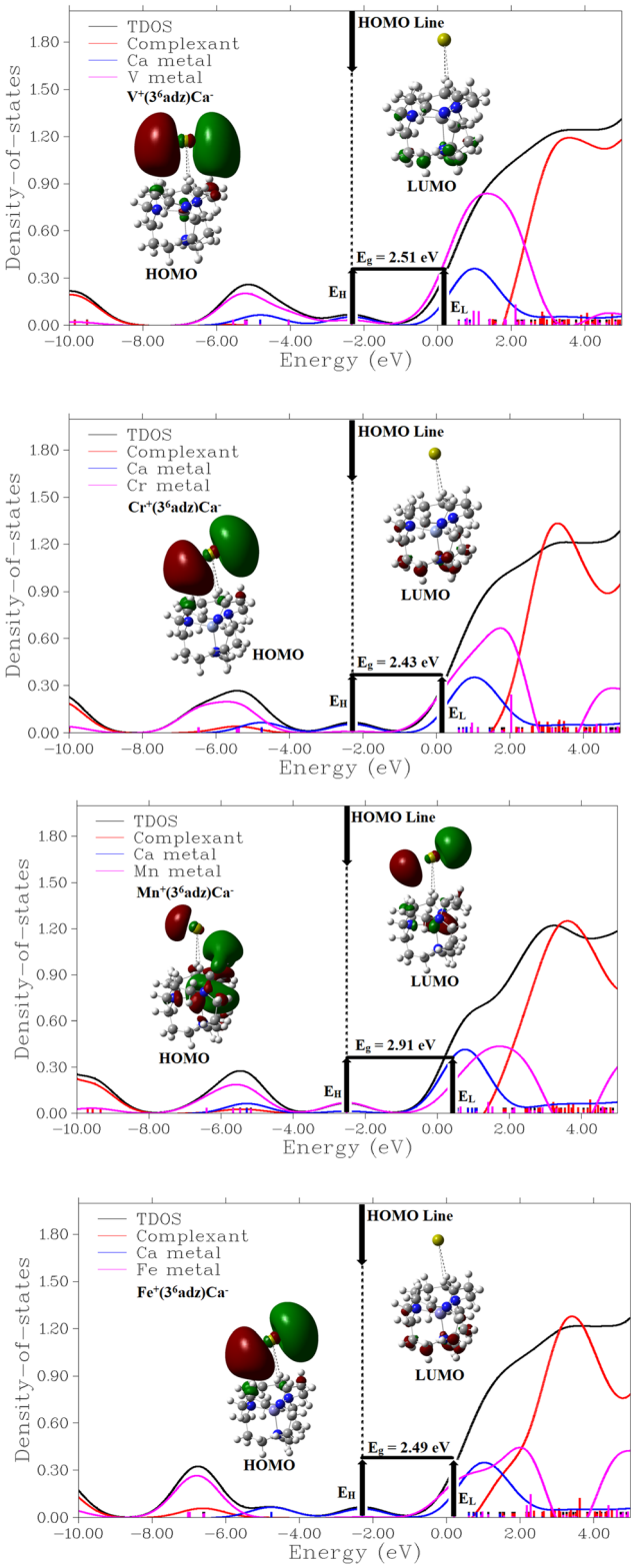

Fig. 5 PDOS spectra of the $M^{+}(3^{6}adz)Ca^{-}$ (M^{+} = V–Zn) series generated using the Multiwfn software.

dipole moment changes in a nonlinear pattern due to unsymmetrical variations in the interaction distance between the charges and the magnitude of the charges over the acceptor metal. Although the same trend is not present in the dipole moment values and the distance between the doped metals, along with the NBO charges on both metals, one can clearly observe the decrease in the dipole moment values with the decrease in the interaction distance and the NBO charges. Also, μ_o increases with increases in the distance between the intercalated metals and charges over the acceptor metals. Thus, the distance between the charges and the NBO charges over the intercalated metals (especially over the acceptor metals) is the major factor that controls the dipole moment.

3.3. Nonlinear optical response of the complexes

In the studied complexes, the electrons of the transition metals are pushed outwards and become localized around the Ca metal, where they behave as excess electrons. These loosely bound electrons can be readily excited to higher energy states with relatively low excitation energy, which contributes to the enhanced nonlinear optical (NLO) response of the systems. Therefore, the NLO properties of the designed complexes were investigated, and the calculated polarizability (α_o) and hyperpolarizability (β_o) values are shown in Table 2. The polarizability is referred to as the ability of a molecule to generate a dipole moment in response to an external field. It measures how the electronic cloud is distorted in complexes. It is found that the polarizability changes in a non-monotonic order. The trend of polarizability observed is: $Zn^{+}(3^{6}adz)Ca^{-}$ (4729 a.u.) > $Mn^{+}(3^{6}adz)Ca^{-}$ (902 a.u.) > $V^{+}(3^{6}adz)Ca^{-}$ (721 a.u.) > $Fe^{+}(3^{6}adz)Ca^{-}$ (672 a.u.) = $Cr^{+}(3^{6}adz)Ca^{-}$ (672 a.u.) > $Ni^{+}(3^{6}adz)Ca^{-}$ (671 a.u.) > $Cu^{+}(3^{6}adz)Ca^{-}$ (665 a.u.) > $Co^{+}(3^{6}adz)Ca^{-}$ (663 a.u.). This irregular trend indicates that polarizability cannot be explained solely based on atomic size. Although the atomic size generally decreases from V to Zn across the period, α_o is primarily governed by electronic factors, such as d-orbital configuration, extent of charge transfer, the interaction distance between the metal centers, and the degree of electron cloud delocalization. The gradual decrease in α_o from V to Ni can be partially associated with reduced atomic size and interaction distance; however, this is not the dominant factor. On the other hand, $Zn^{+}(3^{6}adz)Ca^{-}$ exhibits a larger value of α_o in the presented series, which is attributed to its fully filled d^{10} electronic configuration, enhanced orbital polarization, and greater electronic softness. These features generate significant distortion of the electron cloud, leading to increased polarizability. Therefore, the observed variation in α_o arises from a combination of structural and electronic effects rather than atomic size alone.

Furthermore, the first β_o of the $M^{+}(3^{6}adz)Ca^{-}$ series also changes in non-monotonic order (as shown in Table 2). This happens due to non-monotonic changes in the size of the TMs and the interaction distance between the metals in the complexes. The observed β_o is in order of $Zn^{+}(3^{6}adz)Ca^{-}$ (3.17×10^{6} a.u.) > $Mn^{+}(3^{6}adz)Ca^{-}$ (1.96×10^{5} a.u.) > $V^{+}(3^{6}adz)Ca^{-}$ (1.38×10^{5} a.u.) > $Fe^{+}(3^{6}adz)Ca^{-}$ (5.93×10^{4} a.u.) > $Cu^{+}(3^{6}adz)Ca^{-}$ (5.80×10^{4} a.u.) > $Cr^{+}(3^{6}adz)Ca^{-}$ (5.29×10^{4} a.u.) > $Ni^{+}(3^{6}adz)Ca^{-}$ (5.19×10^{4} a.u.) > $Co^{+}(3^{6}adz)Ca^{-}$ (4.21×10^{4} a.u.). In this series, the $Zn^{+}(3^{6}adz)Ca^{-}$ shows the highest β_o, along with higher polarizability due to the smaller E_{H-L} gap and greater size of Zn, which leads to higher polarization in the complex.

Table 2 Polarizability (α_o) in a.u., first hyperpolarizability (β_o) in a.u., projection of hyperpolarizability (β_{vec}) in a.u., λ_{max} in nm, excitation energy (ΔE) in eV, oscillation strength (f_o) in a.u. and change in dipole moment ($\Delta\mu$) in Debye of the $M^+(3^6adz)Ca^-$ (M^+ = V–Zn) series

$M^+(3^6adz)Ca^-$	α_o	β_o	β_{vec}	λ_{max}	ΔE	f_o	$\Delta\mu$
$V^+(3^6adz)Ca^-$	721	1.38×10^5	3.37×10^3	1658	0.74	0.10	1.74
$Cr^+(3^6adz)Ca^-$	672	5.29×10^4	6.40×10^3	543	2.28	0.13	3.85
$Mn^+(3^6adz)Ca^-$	902	1.96×10^5	5.49×10^2	1405	0.88	0.08	6.38
$Fe^+(3^6adz)Ca^-$	672	5.93×10^4	4.38×10^1	1631	0.76	0.07	0.079
$Co^+(3^6adz)Ca^-$	663	4.21×10^4	5.75×10^1	1586	0.78	0.08	0.26
$Ni^+(3^6adz)Ca^-$	671	5.19×10^4	1.15×10^1	1628	0.76	0.08	0.10
$Cu^+(3^6adz)Ca^-$	665	5.80×10^4	1.76×10^4	543	2.28	0.12	3.81
$Zn^+(3^6adz)Ca^-$	4729	3.17×10^6	9.86×10^3	1833	0.67	0.31	13.15

The enhanced NLO response of the $Zn^+(3^6adz)Ca^-$ complex can also be associated with the fully filled d^{10} electronic configuration of the Zn, which provides greater electronic softness and facilitates efficient polarization of the electron cloud. The closed-shell nature of Zn reduces electron–electron repulsion and promotes charge redistribution toward the Ca center, thereby enhancing the hyperpolarizability. In contrast, the relatively high NLO response of $Mn^+(3^6adz)Ca^-$ arises from its half-filled d^5 electronic configuration, which generates a spin-polarized electronic structure and promotes asymmetry in charge distribution. This facilitates intramolecular charge transfer and contributes significantly to the enhanced polarizability and first hyperpolarizability of the Mn complex. On the other hand, the $Co^+(3^6adz)Ca^-$ complex shows the lowest β_o value in the Ca series due to the smaller atomic size of cobalt. So, in this case, electrons are not easily transferred toward the Ca metal (lower charge transfer), and the H–L gap is quite high, which decreases the β_o slightly.

3.4. Factors governing hyperpolarizability

There are many factors that affect the hyperpolarizabilities of complexes, *i.e.*, oscillation strength (f_o), change in dipole moment ($\Delta\mu$), and excitation energy (ΔE) (energy needed to excite electrons from the ground state to the excited state). All these parameters were calculated by using a two-level model analysis (eqn (8)), and the values are presented in Table 2.

$$\beta_{TL} = \frac{\Delta\mu \times f_o}{(\Delta E)^3} \quad (8)$$

where β_{TL} is the first hyperpolarizability estimated using the two-level model, $\Delta\mu$ is the change in dipole moment between the ground and excited states, f_o is the oscillator strength, and ΔE is the transition energy. Eqn (8) shows the direct relation of hyperpolarizability with f_o and $\Delta\mu$, but an inverse relation with ΔE. All the essential transitions are determined by employing the TD-DFT approach. The inverse relationship of β_o and ΔE can be observed from the results of β_o (up to 10^6 a.u.) and the small values of ΔE (0.67 eV to 2.28 eV) for the studied complexes. These calculated small values of ΔE are a prime reason behind the elevated hyperpolarizability (as stated in the literature).[49,73–75] Furthermore, the inverse relation of β_o and ΔE can be observed by looking at the results obtained for $M^+(3^6adz)Ca^-$. The analysis reveals that the β_o of the complexes rises with the reduction of ΔE. The $Zn^+(3^6adz)Ca^-$ complex exhibits the highest β_o in the presented series, which is attributed to the smaller excitation energy (0.67 eV) of the Zn-containing complex. So, electrons become loosely attached and excite easily, which enhances the hyperpolarizability of the complex. The lowest hyperpolarizability is calculated for $Co^+(3^6adz)Ca^-$ due to its relatively high ΔE value (0.78 eV), along with low oscillator strength and a small change in dipole moment for the same complex. This happens because when Co metal interacts with Ca metal in the complex, it undergoes a change in oxidation state, making it more stable; thus, it shows a lower NLO response. Additionally, the resulting structure of Co after interaction with Ca metal is different and restricts the movement of electrons in it, which ultimately reduces its hyperpolarizability.

Additionally, according to the two-level model, oscillator strength (f_o) is one of the important contributing parameters governing β_o. The $M^+(3^6adz)Ca^-$ series indicates that complexes possessing higher f_o values along with favorable ΔE and $\Delta\mu$ values exhibit enhanced hyperpolarizability (Table 2). The $V^+(3^6adz)Ca^-$ (1.38×10^5 a.u.) and $Zn^+(3^6adz)Ca^-$ (3.17×10^6 a.u.) have higher hyperpolarizability in the investigated series due to greater values of oscillation strength, *i.e.*, 0.10 and 0.31, respectively.

Furthermore, the direct relationship of β_o with $\Delta\mu$ can also be evaluated from the results of the $M^+(3^6adz)Ca^-$ series, where higher hyperpolarizability values of 3.17×10^6 and 1.96×10^5 a.u. are calculated for the $Zn^+(3^6adz)Ca^-$ and $Mn^+(3^6adz)Ca^-$ complexes, respectively, along with quite high dipole moment ($\Delta\mu$) values of 13.15 and 6.38 D, respectively, in the series.

The other factor to predict the NLO response of a material accurately is the β_{vec} value. It represents the projection of the first hyperpolarizability over the dipole moment vector.[76] In the current study, the β_{vec} values of TMs and Ca metal-doped complexes were analyzed, and the results are presented in Table 2. The vector dipoles of both metals in the studied complexes are found over the *x*-axis. The computed β_{vec} values are slightly smaller than the first hyperpolarizability values, which suggests that the projection of the hyperpolarizability and dipole moment vectors lies in the same direction, ensuring the unidirectional flow of charge parallel to the *x*-axis in these complexes.

3.5. Absorption (UV-vis-NIR) analysis

The UV-visible absorption spectra of the $M^+(3^6adz)Ca^-$ series of complexes were calculated and are shown in Fig. 6/S4. These complexes exhibit absorption mainly in the infrared region, except for $Cr^+(3^6adz)Ca^-$ and $Cu^+(3^6adz)Ca^-$, which show

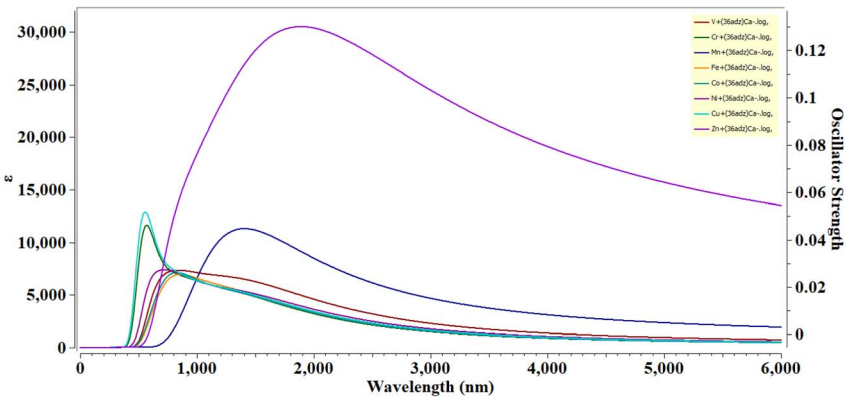

Fig. 6 UV absorption spectra of the $M^+(3^6adz)Ca^-$ (M^+ = V to Zn) series.

absorptions in the visible region (Table 2). The λ_{max} values vary non-linearly across the series due to changes in excitation energy (ΔE), HOMO–LUMO gap, and oscillator strength. The $V^+(3^6adz)Ca^-$ shows absorption at 1658 nm due to lower excitation energy, while $Cr^+(3^6adz)Ca^-$ exhibits a blue shift at 543 nm due to higher ΔE. $Mn^+(3^6adz)Ca^-$ and $Fe^+(3^6adz)Ca^-$ show red-shifted absorption due to the reduced excitation energy, while $Co^+(3^6adz)Ca^-$ absorbs at 1586 nm due to a slight increase in the ΔE and energy gap. The $Cu^+(3^6adz)Ca^-$ complex shows absorption at 543 nm, while $Zn^+(3^6adz)Ca^-$ exhibits the highest λ_{max} (1833 nm) due to the low excitation energy and oscillation strength.

Overall, the complexes with lower λ_{max} values possess higher excitation energies. While those with higher λ_{max} show the lower ΔE, *i.e.*, $Zn^+(3^6adz)Ca^-$. These results confirm that the studied complexes are transparent in the UV region.

3.6. Effect of EEF on $M^+(3^6adz)Ca^-$

After analyzing the NLO response of the $M^+(3^6adz)Ca^-$ series, we aligned the TMs and Ca complexes along the *x*-axis using the VMD (Visual Molecular Dynamics) software for the application of EEF in a precise direction, *i.e.*, $\pm x$ axis (as shown in Fig. 7).

This results in applying the EEF from M^+ to Ca^-, and in the opposite direction, *i.e.*, from Ca^- to M^+, along the *x*-axis in the investigated complexes. After optimization, a detailed study of the FMO, NBO, and hyperpolarizability was carried out under the influence of an EEF of 0.001 a.u. strength to estimate the changes in E_{H-L}, polarizability, charges magnitude over both metals, and the hyperpolarizability of the complexes. After employing EEF, we got surprising results (represented in Table 3 and 4).

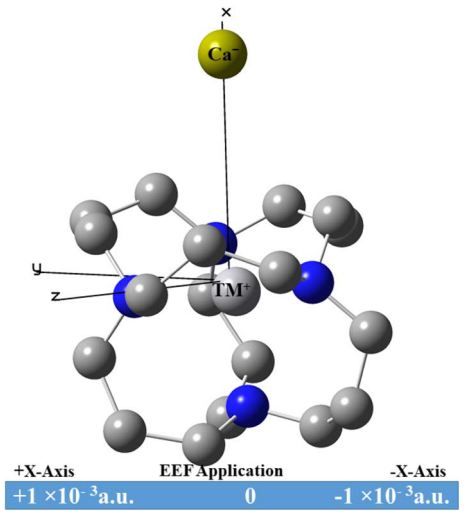

Fig. 7 Structure of the $M^+(3^6adz)Ca^-$ series without the hydrogen atoms and under the effect of an EEF of 10^{-3} a.u. strength, with the direction of the EEF (positive and negative) and the Cartesian axes.

Table 3 Comparison of the NBO charges and energy gaps in the absence and presence of an EEF

Complexes	EEF = 0		EEF = +1 × 10^{-3}		EEF = 0	EEF = +1 × 10^{-3}
$M^+(3^6adz)Ca^-$	Q^+	Q^-	Q^+	Q^-	E_{H-L}	E_{H-L}
$V^+(3^6adz)Ca^-$	0.07	−0.71	0.08	−0.77	2.51	2.78
$Cr^+(3^6adz)Ca^-$	0.18	−0.74	0.16	−0.68	2.43	2.75
$Mn^+(3^6adz)Ca^-$	0.26	−0.73	0.12	−0.27	2.91	4.97
$Fe^+(3^6adz)Ca^-$	0.24	−0.75	0.22	−0.68	2.49	2.79
$Co^+(3^6adz)Ca^-$	0.30	−0.74	0.27	−0.68	2.55	2.85
$Ni^+(3^6adz)Ca^-$	0.36	−0.76	0.11	−0.12	2.54	2.83
$Cu^+(3^6adz)Ca^-$	0.43	−0.75	0.41	−0.69	2.48	2.79
$Zn^+(3^6adz)Ca^-$	0.52	−0.44	1.12	−0.93	1.70	1.76

Table 4 Comparison of the mean polarizability, first hyperpolarizability and dipole moment results

Complex	EEF = 0			EEF = +1 × 10^{-3} a.u.		
$M^+(3^6adz)Ca^-$	α_o	β_o	μ_o	α_o	β_o	μ_o
$V^+(3^6adz)Ca^-$	721	1.38×10^5	19.46	743	2.90×10^5	21.65
$Cr^+(3^6adz)Ca^-$	672	5.29×10^4	21.31	658	2.09×10^5	26.56
$Mn^+(3^6adz)Ca^-$	902	1.96×10^5	10.57	1131	5.01×10^5	14.02
$Fe^+(3^6adz)Ca^-$	672	5.93×10^4	21.36	650	2.09×10^5	26.69
$Co^+(3^6adz)Ca^-$	663	4.21×10^4	20.97	643	1.98×10^5	26.24
$Ni^+(3^6adz)Ca^-$	671	5.19×10^4	21.21	642	2.02×10^5	26.72
$Cu^+(3^6adz)Ca^-$	665	5.80×10^4	21.43	640	2.07×10^5	26.78
$Zn^+(3^6adz)Ca^-$	4729	3.17×10^6	8.16	2528	1.25×10^7	27.71

Table 4 indicates that a linear increase in the hyperpolarizability of the complexes occurs after employing the EEF. Every complex shows an increase in the hyperpolarizability due to the enhancement of the dipole moment in each complex of the $M^+(3^6adz)Ca^-$ series. The maximum increase in hyperpolarizability is seen for the $Zn^+(3^6adz)Ca^-$ complex; *i.e.*, from 3.17×10^6 to 1.25×10^7 a.u. This increase in hyperpolarizability is credited to an increase in the dipole moment and NBO charge transfer in the same complex. So, the application of EEF is an excellent strategy for designing materials with an elevated NLO response.

4. Conclusion

The strategies to design alkalides with exceptional NLO response are well developed in the literature. On the other hand, alkaline earthides are quite rare due to the low electron affinity of AEMs (alkaline earth metals). In the present study, the geometric, nonlinear, and electronic properties of eight different alkaline earthides, *i.e.*, $M^+(3^6adz)Ca^-$, are investigated. Their design involved carefully doping TMs (V–Zn) on the inner side of 3^6adz, which acts as a donor of excess electrons, and Ca metal outside the cage, which acts as an acceptor of electrons. Then, the alkaline earthide identities of the complexes were verified through NBO and FMO analyses. The complexes are characterized by a negative charge over the Ca metal and localization of the HOMO in the p-orbital over the Ca metal. The earthide nature is further validated by the partial density of states (PDOS) spectra. Furthermore, these features award the complexes with lower values of transition energies, *i.e.*, 0.67 eV to 2.28 eV. These complexes exhibit large NLO responses, with first-hyperpolarizability ranging from 4.21×10^4 to 3.17×10^6 a.u. (the highest calculated value is 3.17×10^6 a.u. for $Zn^+(3^6adz)Ca^-$). Additionally, employing EEF on the complexes results in an excellent increase in hyperpolarizability. An excellent enhancement in the hyperpolarizability of $Zn^+(3^6adz)Ca^-$, *i.e.*, from 3.17×10^6 a.u. to 1.25×10^7 a.u., was calculated after applying an external electric field of 0.001 a.u. strength.

Author contributions

Investigation and writing – original draft: Jabir Hussain; supervision: Riaz Hussain; formal analysis and data curation: Dua Tahreem; writing – review and editing: Annum Ahsan; supervision and formal analysis: Muhammad Arshad; and resources and software: Khurshid Ayub.

Conflicts of interest

All authors declare no financial or non-financial competing interests.

Abbreviations

AEMs	Alkaline earth metals
AMs	Alkali metals
DF:	Density functional theory
TD-DFT	Time-dependent density functional theory
NLO	Nonlinear optical
HOMO	Highest occupied molecular orbital
LUMO	Lowest unoccupied molecular orbital
PDOS	Partial density of states
NBO	Natural bond orbital
EEF	External electric field
VIP	Vertical ionization potential
α_o	Polarizability
β_o	First hyperpolarizability
β_{vec}	Projection of hyperpolarizability
ΔE	Excitation energy
$\Delta\mu$	Change in dipole moment
f_o	Oscillator strength

Data availability

Data will be made available upon request.

Supplementary information (SI): PDOS sepctra, HOMO and LUMO of $M^+(3^6adz)Ca^-$ (here M^+ is Co to Zn) along with individual UV graph of each complex. See DOI: https://doi.org/10.1039/d6ra02261h.

References

1 S. Ju, P. R. Watekar, S. Jeong, Y. Kim and W.-T. Han, *J. Nonlinear Opt. Phys. Mater.*, 2010, **19**, 791–799.
2 T. Jiang, G. Qin, W. Qin and J. Zhou, *Optik*, 2014, **125**, 5789–5793.
3 P. Ren, H. Fan and X. Wang, *Catal. Commun.*, 2012, **25**, 32–35.
4 S. Muhammad, M. Nakano, A. G. Al-Sehemi, Y. Kitagawa, A. Irfan, A. R. Chaudhry, R. Kishi, S. Ito, K. Yoneda and K. Fukuda, *Nanoscale*, 2016, **8**, 17998–18020.
5 S. Winter, N. Tortik, A. Kubin, B. Krammer and K. Plaetzer, *Photochem. Photobiol. Sci.*, 2013, **12**, 1795–1802.
6 S. Muhammad and M. Nakano, *Nanoscience Comput. Chem. Res. Prog.*, 2013, 309.
7 S. Trabelsi, N. Issaoui, S. A. Brandán, F. Bardak, T. Roisnel, A. Atac and H. Marouani, *J. Mol. Struct.*, 2019, **1185**, 168–182.
8 A. Sagaama, N. Issaoui, O. Al-Dossary, A. S. Kazachenko and M. J. Wojcik, *J. King Saud Univ. Sci.*, 2021, **33**, 101606.
9 A. Ramalingam, S. Sambandam, M. Medimagh, O. Al-Dossary, N. Issaoui and M. J. Wojcik, *J. King Saud Univ. Sci.*, 2021, **33**, 101632.
10 M. Nakano, R. Kishi, T. Nitta, T. Kubo, K. Nakasuji, K. Kamada, K. Ohta, B. Champagne, E. Botek and K. Yamaguchi, *J. Phys. Chem.*, 2005, **109**, 885–891.
11 M. Nakano, T. Kubo, K. Kamada, K. Ohta, R. Kishi, S. Ohta, N. Nakagawa, H. Takahashi, S.-i. Furukawa, Y. Morita, K. Nakasuji and K. Yamaguchi, *Chem. Phys. Lett.*, 2006, **418**, 142–147.
12 J. Abe, Y. Shirai, N. Nemoto and Y. Nagase, *J. Phys. Chem.*, 1997, **101**, 1–4.

13 Y. Liu, X. Xu, F. Zheng and Y. Cui, *Angew. Chem.*, 2008, **120**, 4614–4617.
14 R.-L. Zhong, H.-L. Xu, Z.-R. Li and Z.-M. Su, *J. Phys. Chem. Lett.*, 2015, **6**, 612–619.
15 N. Kosar, K. Shehzadi, K. Ayub and T. Mahmood, *J. Mol. Graph. Model.*, 2020, **97**, 107573.
16 N. Kosar, T. Mahmood, K. Ayub, S. Tabassum, M. Arshad and M. A. Gilani, *Opt Laser. Technol.*, 2019, **120**, 105753.
17 F. Ullah, N. Kosar, K. Ayub and T. Mahmood, *Appl. Surf. Sci.*, 2019, **483**, 1118–1128.
18 G. Yu, X. Huang, S. Li and W. Chen, *Int. J. Quantum Chem.*, 2015, **115**, 671–679.
19 J. J. Wang, Z. J. Zhou, Y. Bai, H. M. He, D. Wu, Y. Li, Z. R. Li and H. X. Zhang, *Dalton Trans.*, 2015, **44**(9), 4207–4214.
20 M. Miyakawa, S. W. Kim, M. Hirano, Y. Kohama, H. Kawaji, T. Atake, H. Ikegami, K. Kono and H. Hosono, *J. Am. Chem. Soc.*, 2007, **129**, 7270–7271.
21 H. E. Nistazakis, A. N. Stassinakis, S. Sheikh Muhammad and G. S. Tombras, *Opt Laser. Technol.*, 2014, **64**, 106–112.
22 W. Chen, Z.-R. Li, D. Wu, F.-L. Gu, X.-Y. Hao, B.-Q. Wang, R.-J. Li and C.-C. Sun, *J. Chem. Phys.*, 2004, **121**, 10489–10494.
23 Y. Li, Z.-R. Li, D. Wu, R.-Y. Li, X.-Y. Hao and C.-C. Sun, *J. Phys. Chem. B*, 2004, **108**, 3145–3148.
24 K. Ayub, *J. Mater. Chem. C*, 2016, **4**, 10919–10934.
25 F. Ullah, N. Kosar, M. N. Arshad, M. A. Gilani, K. Ayub and T. Mahmood, *Opt Laser. Technol.*, 2020, **122**, 105855.
26 A. S. Rad and K. Ayub, *Mater. Res. Bull.*, 2018, **97**, 399–404.
27 M. J. Wagner and J. L. Dye, *J. Solid State Chem.*, 1995, **117**, 309–317.
28 R. Huang, M. Faber, K. Moeggenborg, D. Ward and J. Dye, *Nature*, 1988, **331**, 599–601.
29 M. J. Wagner, R. H. Huang, J. L. Eglin and J. L. Dye, *Nature*, 1994, **368**, 726–729.
30 M. Y. Redko, J. E. Jackson, R. H. Huang and J. L. Dye, *J. Am. Chem. Soc.*, 2005, **127**, 12416–12422.
31 W. Chen, Z.-R. Li, D. Wu, Y. Li, C.-C. Sun and F. L. Gu, *J. Am. Chem. Soc.*, 2005, **127**, 10977–10981.
32 X. Li, *J. Mater. Chem. C*, 2018, **6**, 7576–7583.
33 A. S. Ichimura, M. J. Wagner and J. L. Dye, *J. Phys. Chem. B*, 2002, **106**, 11196–11202.
34 W. M. Sun, Y. Li, X. H. Li, D. Wu, H. M. He, C. Y. Li, J. H. Chen and Z. R. Li, *ChemPhysChem*, 2016, **17**, 2672–2678.
35 X.-H. Li, L. Zhang, X.-L. Zhang, B.-L. Ni, C.-Y. Li and W.-M. Sun, *New J. Chem.*, 2020, **44**, 6411–6419.
36 W.-M. Sun, L.-T. Fan, Y. Li, J.-Y. Liu, D. Wu and Z.-R. Li, *Inorg. Chem.*, 2014, **53**, 6170–6178.
37 W.-M. Sun, D. Wu, Y. Li and Z.-R. Li, *Dalton Trans.*, 2014, **43**, 486–494.
38 W.-M. Sun, D. Wu, Y. Li, J.-Y. Liu, H.-M. He and Z.-R. Li, *Phys. Chem. Chem. Phys.*, 2015, **17**, 4524–4532.
39 W. Chen, Z.-R. Li, D. Wu, Y. Li, C.-C. Sun, F. L. Gu and Y. Aoki, *J. Am. Chem. Soc.*, 2006, **128**, 1072–1073.
40 F.-F. Wang, Z.-R. Li, D. Wu, B.-Q. Wang, Y. Li, Z.-J. Li, W. Chen, G.-T. Yu, F. L. Gu and Y. Aoki, *J. Phys. Chem. B*, 2008, **112**, 1090–1094.
41 J. Hou, D. Jiang, J. Qin and Q. Duan, *Chem. Phys. Lett.*, 2018, **711**, 55–59.
42 A. Ahsan, S. Sarfaraz, F. Fayyaz, M. Asghar and K. Ayub, *Mater. Sci. Semicond. Process.*, 2023, **153**, 107119.
43 A. Ahsan and K. Ayub, *Opt Laser. Technol.*, 2020, **129**, 106298.
44 A. Ahsan, S. Sarfaraz, F. Fayyaz, M. Asghar and K. Ayub, *J. Mol. Liq.*, 2022, **350**, 118504.
45 A. Ahsan, S. Sarfaraz, M. A. Gilani, T. Mahmood, Z. Ahmad and K. Ayub, *Eur. Phys. J. Plus*, 2022, **137**, 1149.
46 A. Ahsan and K. Ayub, *J. Mol. Liq.*, 2020, **297**, 111899.
47 J. Hussain, R. Hussain, A. Hussain, M. A. Yawer, M. Arshad, S. S. Alarfaji, A. Rauf and K. Ayub, *J. Mol. Graph. Model.*, 2024, **130**, 108791.
48 A. Rasool, S. Zahid, A. Elmushyakhi, M. Ans, A. M. Shawky, K. Ayub and J. Iqbal, *Phys. Scr.*, 2023, **98**, 025504.
49 W.-M. Sun, X. Cheng, W.-L. Wang and X.-H. Li, *Organometallics*, 2022, **41**, 2406–2414.
50 Y.-L. Ye, K.-Y. Pan, B.-L. Ni and W.-M. Sun, *Front. Chem.*, 2022, **10**, 853160.
51 M. Savarese, E. Bremond and C. Adamo, *Theor. Chem. Acc.*, 2016, **135**, 1–11.
52 S. Grimme, J. Antony, S. Ehrlich and H. Krieg, *J. Chem. Phys.*, 2010, **132**(15), 154104.
53 S. Grimme, *J. Comput. Chem.*, 2004, **25**, 1463–1473.
54 L. Xu, A. Kumar and B. M. Wong, *J. Comput. Chem.*, 2018, **39**, 2350–2359.
55 H.-Q. Wang, J.-T. Ye, Y. Zhang, Y.-Y. Zhao and Y.-Q. Qiu, *J. Mater. Chem. C*, 2019, **7**, 7531–7547.
56 H.-Q. Wang, L. Wang, Y.-Y. Xia, J.-T. Ye, H.-Y. Zhao and Y.-Q. Qiu, *J. Phys. Chem. C*, 2017, **121**, 16470–16480.
57 H.-Q. Wang, L. Wang, J.-T. Ye, H.-M. Xie and Y.-Q. Qiu, *J. Phys. Chem. C*, 2017, **121**, 28462–28474.
58 F. Ullah, K. Ayub and T. Mahmood, *New J. Chem.*, 2020, **44**, 9822–9829.
59 S. Wajid, N. Kosar, F. Ullah, M. A. Gilani, K. Ayub, S. Muhammad and T. Mahmood, *ACS Omega*, 2021, **6**, 29852–29861.
60 N. Kosar, K. Ayub and T. Mahmood, *J. Mol. Graph. Model.*, 2021, **102**, 107794.
61 M. Frisch, G. Trucks, H. Schlegel, G. Scuseria, M. Robb, J. Cheeseman, G. Scalmani, V. Barone, B. Mennucci and G. Petersson, *Revision D. 01, Gaussian*, Gaussian Inc., Wallingford CT, 2009.
62 S. Khan, M. Yar, N. Kosar, K. Ayub, M. Arshad, M. N. Zahid and T. Mahmood, *Comput. Theor. Chem.*, 2020, **1191**, 113043.
63 A. A. Soliman, A. M. Sayed, O. I. Alajrawy and W. Linert, *J. Mol. Struct.*, 2017, **1137**, 453–460.
64 O. I. Alajrawy and A. A. Almhmdi, *J. Mol. Struct.*, 2022, **1260**, 132813.
65 O. I. Alajrawy, H. A. Hadi, R. S. Awad Al-Luhaibi and B. A. Sabbar, *Results Chem.*, 2023, **5**, 100712.
66 T. Lu and F. Chen, *J. Comput. Chem.*, 2012, **33**, 580–592.
67 J. Hussain, R. Hussain, A. Hussain, A. Ahsan, M. Arshad, K. F. Fawy and K. Ayub, *Struct. Chem.*, 2026, **37**, 463–479.
68 J. Hussain, R. Hussain, A. Hussain, M. Arshad, M. D. S. Haider, K. F. Fawy, R. S. Ahmed, M. Zahra and K. Ayub, *Polyhedron*, 2025, 117711.

69 J. Hussain, R. Hussain, A. Hussain, M. A. Yawer, M. Arshad, S. S. Alarfaji, A. Rauf and K. Ayub, *J. Mol. Graph. Model.*, 2024, 108791.
70 J. Hussain, R. F. Mehmood, R. Hussain, S. Tariq, M. Farooq, M. Arshad, A. Hussain and K. Ayub, *Struct. Chem.*, 2026, DOI: 10.1007/s11224-025-02718-w.
71 T. T. Ahmed and O. I. Alajrawy, *Mater. Today: Proc.*, 2023, **80**, 3823–3836.
72 A. A. Soliman, F. A. Attaby, O. I. Alajrawy and S. R. Majeed, *J. Therm. Anal. Calorim.*, 2019, **135**, 2457–2473.
73 W.-M. Sun, X.-H. Li, J. Wu, J.-M. Lan, C.-Y. Li, D. Wu, Y. Li and Z.-R. Li, *Inorg. Chem.*, 2017, **56**, 4594–4600.
74 W.-M. Sun, B.-L. Ni, D. Wu, J.-M. Lan, C.-Y. Li, Y. Li and Z.-R. Li, *Organometallics*, 2017, **36**, 3352–3359.
75 W.-M. Sun, X.-H. Li, Di Wu, Y. Li, H.-M. He, Z.-R. Li, J.-H. Chen and C. Y. Li, *Dalton Trans.*, 2016, **45**, 7500–7509.
76 B. G. Kim and H. J. Choi, *Phys. Rev. B Condens. Matter*, 2012, **86**, 115435.